Evaluation of the Healing Potential of Silicon Carbide/Bioactive Glass/Carboxymethyl Chitosan Nanocomposites on Extraction Socket in Albino Rats

Original Article

Mai A. Ragab[1], Dina B.E. Farag[1], Zeinab A. Salem[1,2], Hanan H. Beherei[3] and Sahar M. Shawkat[1]

[1]*Department of Oral Biology, Faculty of Dentistry, Cairo University, Cairo, Egypt.*

[2]*Faculty of Oral and Dental Medicine, October 6 University, Giza, Egypt.*

[3]*Department of Ceramics and Building Materials, Advanced Materials Technology and Mineral Resources Research Institute, National Research Center.*

ABSTRACT

Introduction: Dental extraction is one of the most widely performed dental procedures. Delayed healing is reported to occur in less than 11% of all extraction. The aim of this study was to evaluate the healing potential of silicon carbide/bioactive glass/carboxymethyl chitosan nanocomposites on extraction socket of albino rats.

Materials and Methods: 36 male Albino rats were used in this study. Bilateral extraction of first mandibular molars was done. The rats were randomly assigned into four groups, GI: Control group; without treatment, GII: Carboxy-methyl chitosan group (CMC), GIII: Silicon carbide/Bioactive glass group(SiC/BG) and GIV: Silicon Carbide/Bioactive Glass/Carboxymethyl Chitosan (SiC/BG/CMC). Each group was divided according to the date of sacrifice 3,7 and 14 days into three subgroups. Healing efficacy of the materials were evaluated histologically, histomorphometricaly and by using real time polymerase chain reaction (qRT-PCR) for quantitative analysis of osteopontin (OPN) gene expression. Statistical analysis for all data was performed.

Results: Histological results revealed group I showed a slower healing rate than other groups. Group II exhibited a better healing cascade than group I. Group III and group IV revealed a better healing with more bone formation than other groups at different time intervals. A significant increase in bone area percentage has been recorded in group IV along different experimental periods. Regarding the highest value for immature bone collagen area percentage, it was recorded at 14 days in group II while the lowest value was recorded in group IV at 14 days. qRT-PCR results revealed at 3 and 7 days' interval; a significant increase in OPN level was detected in group II, while at 14 days' interval; the highest OPN level was detected in group IV followed by group III.

Conclusions: SiC/BG/CMC group can have superior results as more mature bone formation with a more regularly arranged osteocytes as compared to other groups.

Received: 24 January 2025, **Accepted:** 06 March 2025

Key Words: Bioactive glasses; carboxymethyl chitosan; extraction sockets; nanocomposites; Silicon carbide.

Corresponding Author: Mai A. Ragab, PhD, Department of Oral Biology, Faculty of Dentistry, Cairo University, Cairo, Egypt, **Tel.**: +20 10 1968 7900, **E-mail:** mai_ali@dentistry.cu.edu.eg

ISSN: 1110-0559, Vol. 48, No. 3

INTRODUCTION

One of the most common dental procedures is dental extraction. Even though they could be avoided, dental cavities and periodontal disease continue to be the most frequent causes of tooth extractions, particularly in underdeveloped countries[1].

After extraction, both the hard and soft tissues heal without any visible complications. Although the healing of extraction sockets is generally a rapid and uncomplicated process, delayed healing, overt infection, or failure of recent exodontia sites to heal can occur. Delayed healing is reported to occur in less than 11% of all extraction[2-4]. Occlusion and long-term preservation of prosthetic function are becoming increasingly difficult because of the deterioration of alveolar bone level. As a result, alveolar crest height must be maintained, as well as rapid wound healing after tooth extraction. This is the basis for the socket preservation concept[5].

A great variety of synthetic and natural biomaterials for socket grafting had been proposed. Carboxymethyl chitosan (CMC), was proved to have the same physical and biological features as chitosan (CS). The presence of a "carboxymethyl" group in the molecular structure gives the CMC better qualities such as sorption, flocculation, chelating, membrane formation, moisture retention and

DOI: 10.21608/ejh.2025.353688.2201

viscosity. Better biological characteristics, such as altered cell function, antibacterial, antiapoptotic and antioxidant activities, were demonstrated by the CMC[6].

One of the promising synthetic biomaterials that has been employed for both soft and hard tissue regeneration is bioactive glasses[7,8]. Because bioactive glass is known to be firmly adhere to bone and promote bone growth in *vivo*, it offers a wide range of uses in bone tissue regeneration. According to in *vitro* studies, the ionic products of bioactive glass disintegration enhanced osteoblast adhesion, differentiation, proliferation and mineralization[9].

Recently, silicon carbide bioceramics provided a promising effect in the biomedical field because of its several advantages, such as its chemical and physical stability, biocompatibility and non-reactivity to the chemicals in the human body. Because of their enhanced biological responses and capacity to accelerate the creation of new bone, bioactive glasses make excellent candidates for coating or base matrix materials in silicon carbide (SiC) ceramics. Clinical research has verified the successful application of these bioactive compounds as a coating on metal alloys using various deposition methods[10,11].

However, the weak mechanical properties of bioactive glass, like its porous architecture, restrict its use in a wide range of applications. Thus, composites are becoming increasingly used in biomedical applications, owing to the powerful blend of the ideal properties of their constituents[9].

Biomaterials at a nanoscale are the focus of nanotechnology. Particles with at least a dimension of 100 nm or smaller are considered nanomaterials. The materials' physico-chemical characteristics vary depending on scale and surface modification, making them appropriate for biomedical uses such as medication delivery, illness diagnosis and treatment[12,13]. Thus, this study was conducted to evaluate the healing potential of Silicon Carbide/Bioactive Glass/Carboxymethyl Chitosan nanocomposites on extraction socket in albino rats.

MATERIAL AND METHODS

Material preparation

Nanocomposite materials

Nanocomposite materials were prepared at biomaterial department, national research center.

All other chemicals were of analytical grade. The SiC powder was purchased from (US Research Nanomaterials, Houston, TX). Tetraethyl orthosilicate (TEOS) Si (OC2H5)4) (99.90% pure) as silicon precursor, calcium nitrate tetrahydrate (99%) as the calcium precursor, sodium hydroxide (NaOH), acetic acid, to promote hydrolysis of calcium silicate glass, mono-chloroacetic acid, tri-polyphosphate (TPP), citric acid monohydrate (99–100%) and absolute ethanol and chitosan (MW = 3.5×10^5, >80% deacetylated) were purchased from Sigma Aldrich.

Preparation of carboxymethyl chitosan hydrogel

Preparation of "carboxymethyl chitosan" (CMC) from chitosan (88%of deacetylation, (5g) solution with 1% (v/v) acetic acid as solvent was added in 20% NaOH solution (100 mL) for 15 min. The monochloroacetic acid (15 g) was added slowly to the mixture and heated at 40 °C for 2 h. The reaction solution was neutralized with 10% acetic acid solution. Therefore, the product was filtered and washed with methanol two times and dried in vacuum at 55 °C for 8 h. NaOH solution and –tri-polyphosphate (TPP) was added to CMC solution gradually under stirring to be gel[14,15].

Preparation of bioactive glass nanoparticles

Bioactive glass-based calcium silicate was prepared with a ratio of 1:1 of Ca: Si, using the following steps: calcium nitrate hexahydrate and tetraethyl orthosilicate (TEOS) Si (OC2H5)4) (99.90% pure) were used, both dissolved in 500 mL of distilled water with absolute ethanol. Then, the two solutions were mixed and stirred for 1 h at room temperature employing a magnetic stirrer. Citric acid monohydrate was used to promote hydrolysis and using ammonium hydroxide as the gelling agent. The solution was kept in a drier at 80°C until gelling. The obtained hard gel was calcined at 600°C for 2 h[16].

Preparation of silicon carbide/bioactive glass/ carboxymethyl Chitosan

SiC/ BG nanopowder was added to CMC solution and the composite was stirred and mixed for 15 min

Physiochemical characterization of the materials

X-ray diffraction (XRD) analysis

The prepared samples underwent X-ray diffraction (XRD) analysis with a BRUKER AXS D8 Advance (Germany). The XRD instrument was equipped with Cu-Kα irradiation and a Ni filter, operating at 40 kV and 40 mA. This technique was employed to assess the impact of the samples' crystallinity or amorphous nature[14].

Fourier Transform Infrared spectroscopy (FTIR)

FT-IR spectra were acquired using a JASCO FTIR-6000 E Fourier transform infrared spectrometer from Japan. The instrument was operated in absorption mode, covering the wave number range of 4000-400 cm-1. The spectra were obtained by mixing the samples with potassium bromide (KBr) discs[15].

TEM

The morphology and size of the prepared bioactive glass nanopowder was examined by a transmission electron microscope (TEM). Specimens were scattered in ethanol and sonicated for 15 min. utilizing an ultrasonic bath. Subsequently, copper grid was submerged in above sonicated systems, dried in air and they were observed by the TEM[17].

Experimental animals

Thirty-six mature male Albino rats weighing between 150 and 200 g and ranging in age from 3 to 4 months were acquired and kept at Cairo University's Faculty of Medicine's animal house. Separate cages with a 12-hour day-night cycle, 24–28°C temperature, and 45–64% humidity were used to house the animals. Before the trial began, all animals were given a semi-purified meal and unlimited access to water for ten days. After teeth extraction, animals were divided into groups based on the Random Sequence Generating Program's (random.org) recommendations.

In accordance with the guidelines and consent of the Faculty of Dentistry's ethical committee on animal experiments, all experimental procedures were carried out in the Faculty of Medicine's animal house at Cairo University in Egypt. (IACUC) (approval no. CU-III -F -3- 22).

Teeth extraction

Sterile extraction was carried out, and intraperitoneal injections of "Xilazin" (Syntec1, 20 mg/kg, IP) and "Ketamine" (Agener1, 40 mg/kg, IP) were used to induce general anesthesia. Bilateral tooth extraction of lower right and left first molars was done in each rat. For extraction, a curved hemostat with a slight buccolingual movement was employed.

Animal Grouping

The rats (n=36) were randomly distributed into four groups (9 rats each) depending on post-extraction treatment (Table 1).

Table 1: showing animal grouping:

Group I (control)	Extraction socket received no treatment	In each group Ia,IIa, IIIa and IVa: Animals were sacrificed after 3 days. Ib,IIb, IIIb and IVa: Animals were sacrificed after 7 days. Ic,IIc, IIIc and IVa: Animals were sacrificed after 14 days.
Group II	Carboxymethyl Chitosan was applied into socket	
Group III	Silicon Carbide/ bioactive glass was applied into socket	
Group IV	Silicon Carbide/bioactive glass/ Carboxy methyl Chitosan nanocomposite was applied into socket	

At each experimental end point, the animals were euthanized by intraperitoneal injection of ketamine overdose (100 mg/kg)[18]. The lower jaws were then dissected and washed in saline solution. The lower jaw specimens comprising the right and left extraction sockets were separated into two halves. For histological analysis, the right side was preserved in 10% neutral buffered formalin. In contrast, the left side was promptly frozen in liquid nitrogen and kept at -80°C for the qRT-PCR analysis.

Histological examination and morphometric analysis

Following cleaning, the samples were submerged in 10% EDTA for four weeks to decalcify them before being washed with distilled water. Specimens were dehydrated in progressively higher alcohol grades before being embedded in paraffin[19]. Five µm thick histological slices were created, put on transparent glass slides, and stained with Hematoxylin and eosin stain (H&E) for regular inspection.

Masson's trichrome was used to identify collagen. It can be applied to highlight collagen specifically in blue (or green, depending on the protocol)[20,21].

Using the image analyzer computer system and image software ("Leica DM LB2 with QWIN Plus image analyzer computer system, Germany"), morphometric analysis was carried out. Using X100 magnification power, the mean area % of bone and immature collagen fibers were determined in five fields per case[22].

Real-time polymerase chain reaction (qRT- PCR)

Osteopontin (OPN) mRNA gene expression was quantitatively measured using the qRT-PCR technique. The SensiFASTTM SYBR® Hi-ROX One-step Kit (Bioline, UK) was used to produce reverse transcription of total RNA into single stranded complementary DNA (cDNA) in a single step, followed by real-time PCR. The reaction mix was made in accordance with the kit's instructions and then used in real-time PCR ("StepOne Applied Biosystem, Foster City, USA"). After the PCR cycles ended, melting curve tests were performed to verify that the expected PCR products were produced precisely. All samples were normalized against GAPDH expression using the ΔCt method. The cycle threshold (Ct) value is the number of qPCR cycles required for the fluorescence signal to exceed a preset threshold. To calculate ΔCt for OPN, GAPDH Ct data were deducted from target RNA Ct values. To calculate ΔΔCt, the ΔCt of the experimental samples was deducted from the ΔCt of the control samples[23].

Statistical analysis

The collected data was coded and entered using the statistical program for the social sciences (SPSS) version 28 (IBM Corp., Armonk, NY, USA). The data was summarized using the mean and standard deviation. Multiple comparison analysis of variance (ANOVA) was used to compare between groups. Post hoc test was done to compare between each two groups[24]. *P-values* less than 0.05 were considered as statistically significant.

RESULTS

Material physicochemical characterizations

X-ray diffraction (XRD) analysis

According to the XRD pattern, the SiC is in the cubic phase and has a high intensity peak close to 2θ = 35:5°,

42.7°, and 60° (CuKa), which is comparable to findings from other research that have already been published. The cell constant α = 4:356 Å, which was obtained after refining, is extremely near to the value for β-SiC that was reported (α = 4:359 Å, JCPDS Card No. 29-1129) (Figure 1). The XRD of the BG based calcium silicate revealed a hump denote the presence an amorphous structure of the glass sample (Figure 2).

Fourier transform infrared spectroscopy (FTIR) results

The most important feature lies in the detection of the stretching mode vibrations of the Si–C bonds, hereafter labeled (Si–C) and located at about 802-820 cm−1, while two additional weak signals are detected in the 1333–1637 cm−1 range. From the infrared spectra, it is clear that the position of the main peak (810–840 cm−1) attributed to (Si–C) is shifted towards high frequencies compared to the stretching mode of the Si–C bond within a crystalline β-SiC phase (790–800 cm−1).

–OH antisymmetric stretching vibration absorption peak (COO) was at 1637-1617 cm−1, –OH symmetrical stretching vibration absorption peak (COO) was at 1433 cm−1, and CMC's C–OH stretching vibration absorption peak was at 1066 cm−1, N–H and O–H at 3404 cm−1 (Figures 3,4).

FTIR studies were performed for Si/BG/CMC nanocomposite; the spectra are given in Figure 4. The spectra of CMC are similar to that of the original chitosan with a new peak appearing at 1637 cm−1, which is assigned to the carbonyl groups. This confirmed the conversion of chitosan to CMC. The characteristic vibration deformation of the primary amine N-H is responsible for the disappearance of the –NH2 associated band at 1452 cm−1 in CMC. Additionally, the quaternary ammonium salt's methyl groups and long carbon segment are responsible for the appearance of some new intense peaks at 2927–2897, 1452, and 802 cm−1. The Si-O Second SiC groups' distinctive peaks arise between 1271 and 1049 cm−1.

Pure CMC's infrared spectra displayed a distinctive broad band at 3260 cm−1 because of the symmetrical stretching vibrations of the –OH and N-H amines. Two brief peaks at 2885 cm−1 and 2826 cm−1 are indicative of stretching vibrations from C to H. The N-H bending of primary amines caused a steep peak to develop at 1579 cm−1, whilst C-N stretching vibrations are responsible for the peak at 1407 cm−1. The C-O stretching vibration is responsible for the distinctive sharp peak at 1320 cm−1. The FTIR spectra of carboxymethyl-chitosan-based nanocarriers showed a comparable peak.

Transmission electron microscope (TEM) results

A fully crystallized SiC grains were appeared slightly agglomerated and surrounded by a very thin transparent layer BG based calcium silicate (~30 nm-50 nm) with clearly visible amorphous grains on the edge of the zone (Figure 5). The contrast appearing within the grey SiC grains exhibits the characteristic features of good crystalline phase on the surface. The ~30 nm grains appear superposed in a large part of the micrograph.

Histopathological results

3 days after extraction:

3 days' post-extraction, the extraction socket of group Ia was almost filled with granulation tissue harboring dissociated immature collagen fibers with massive inflammatory cellular infiltration. Remnants of distorted old lamellar bone with widening in osteocyte lacunae were also observed at the basal portion of the socket (Figures 6A,B).

In group IIa; the socket cavity contained granulation tissue. The granulation tissue was observed to overlies areas of dense fibrous tissue consisting of immature collagen fibers intermingled with mature ones (Figures 6C,D).

In group IIIa; areas of fibrous tissue were evident at the central portion of the socket cavity. Along the base of the socket, newly formed trabecular network of woven bone enclosing numerous osteocytes were seen radiating from old trabecular bone. Areas of intermingling between mature and immature bone trabeculae were clearly observed (Figures 6E,F).

Interestingly, group IVa showed mature and immature collagen fibers that were more prevalent in the fibrous tissue in the central and basal part of the socket. Newly formed woven bone that was in direct contact with remodeled old lamellar bone was evident in the base of the socket (Figures 6G,H).

7 days after extraction

7 days' post-extraction; group Ib showed dense fibrous tissue filling the central part of the socket. Thin rim of newly formed vascularized osteoid matrix was evident basal to the fibrous tissue (Figures 7A,B). Group IIb showed discrete areas of granulation tissue, fibrous tissue as well as osteoid matrix was clearly seen filling the center of the socket together with a fragment of old lamellar bone. Trabecular bone remodeling was observed at the lateral and the basal portions of the socket. The interconnecting bone trabeculae enclosed multiple bone marrow cavities outlined by osteoblastic cells and filled with fibrocellular tissue (Figures 7C,D).

In group IIIb; The base of the socket contained thick bone trabeculae enclosing numerous osteocytes. Areas of immature woven bone was evident among the mature bone trabeculea. Wide highly cellular bone marrow cavities were also observed. Numerous new blood vessels were seen adjacent to bone trabeculae (Figures 7E,F). While group IVb showed partial mucosal epithelial regeneration overlying fibrous lamina propria. Remnants of the graft material were enclosed within the connective tissue. The basal portion of the socket was occupied by thin interconnecting trabeculae of newly formed woven bone

together with old lamellar bone. The woven bone enclosed numerous osteocytes as well as numerous marrow cavities filled with fibrocellular tissue (Figures 7G,H).

14 days after extraction

14 days after extraction; the central and marginal portions of the socket of group Ic were partially filled with dense fibrous tissue overlying network of mineralized bone matrix. Small areas of thin newly formed woven bone were also observed. The basal and lateral portions of the extraction site were characterized by the presence of finger-like projections of remodeled bone trabeculae. The remodeled trabeculae exhibited different patterns of mineralization. Signs of remodeling was clearly revealed by the presence of Howship's lacunae as well as multiple resting and reversal lines. The remodeled bone enclosed multiple irregularly arranged osteocytes where some lacunae were empty. Most of the bone marrow cavities were filled with fibrocellular tissue (Figures 8A,B).

Group IIc showed Immature woven bone intermingled with irregular interconnecting mature bone trabeculae at the base of the socket. The bone trabeculae were seen enclosing wide areas of bone marrow cavities filled with dense fibrocellular tissue. Osteoblasts were clearly seen on the surface of the bone trabeculae. Resting and reversal lines were also observed (Figures 8C,D).

In group IIIc; mature and immature collagen fibers blending together, along with irregular interconnecting bone trabeculae were clearly evident at the base of the socket enclosing numerous entrapped osteocytes as well as various sized bone marrow cavities. Areas of different pattern of mineralization could be seen. Active osteoblasts together with osteoid matrix were also clearly observed at the trabecular bone boundaries. Multiple resting and reversal lines were also detected (Figures 8E,F).

The extraction sockets of group IVc were completely covered with oral mucosa consisted of keratinized epithelium and dense lamina propria. The lateral and basal portion of the socket was occupied by bone that displayed uniform configuration. The bone trabeculae were thick, relatively mature and enclosed orderly arranged osteocytes. Most of the marrow cavities were outlined by osteoblastic cells and filled with fibrocelluar tissue. Active osteoblasts were also seen bordering most of the trabecular boundaries. Interestingly discrete small areas of immature bone trabeculae (woven bone) were still evident. Highly vascular dense fibrous tissue enclosing mature collagen bundles was also observed on top of the formed bone at the central region of the socket (Figures 8G,H).

Histomorphometric results

Bone area percentage (H&E morphometry)

Difference between groups within each time point: The highest value for bone area percentage at 3,7 and 14 days' post extraction was recorded in group IV (SiC/BG/CMC), while the lowest value was recorded in group I (control) with statistically significant difference between groups. Multiple pairwise comparisons between different groups revealed a significantly higher values in groups II (CMC), III (SiC/BG), and IV (SiC/BG/CMC) as compared to group I (control). Moreover, at 3 days, significantly higher values were revealed in groups IIIa and IVa as compared to group IIa. However, the difference between group IVa and group IIIa, was not statistically significant. At 7 and 14 days, significantly higher values were revealed in groups IIIb, IIIc and groups IVb, IVc as compared to groups IIb, IIIc. Additionally, a significant increase was observed in groups IVb, IVc in comparison to groups IIIb, IIIc (Table 2, Figure 9).

Immature bone collagen area percentage

Difference between groups within each time point: At 3and 7 days, the highest value for immature bone collagen area percentage was detected in groups IVa, IVb while the lowest value "was observed in groups Ia, Ib with statistically significant difference between groups. Multiple pairwise comparisons between different groups revealed a significantly higher values in groups II, III, and IV as compared to group I. Moreover, significantly higher values were observed in groups III and IV in comparison to group II. At 3 days', the difference between group IVa and group IIIa, was not statistically significant. However, at 7 days', group IVb had a significant higher value than group IIIb. At 14 days' post-extraction, the highest value for immature bone collagen area percentage was recorded in group IIc while the lowest value was recorded in group IVc with statistically significant difference between groups. Multiple pairwise comparisons showed that, group II had a significantly higher values than group I whereas groups III and IV had a significantly lower values than group I. Similarly, a significantly lower values were detected in groups III and IV as compared to group II, and in group IV compared to group III (Table 3, Figure 10).

Osteopontin (OPN) mRNA gene expression

Difference between groups within each time point: The highest value for OPN gene expression at 3and 7 and 14 days' post-extraction was recorded in group IV, while the lowest value was recorded in group I with statistically significant difference between groups. Multiple pairwise comparisons between different groups observed a significantly higher values in groups II, III, and IV as compared to group I. A significantly higher values were also revealed in groups III, and IV as compared to group II. Moreover, the increase in OPN expression in group IV was significant as compared to group III. (Table 4, Figure 11).

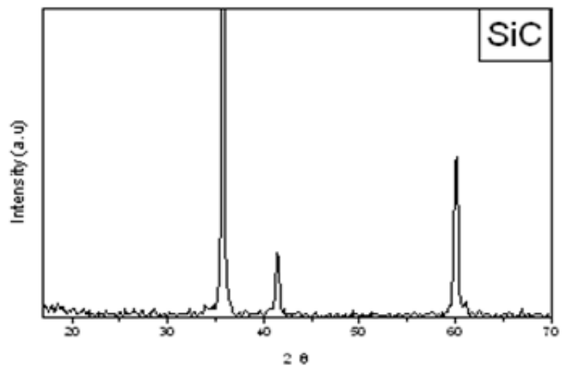

Fig. 1: XRD of SiC

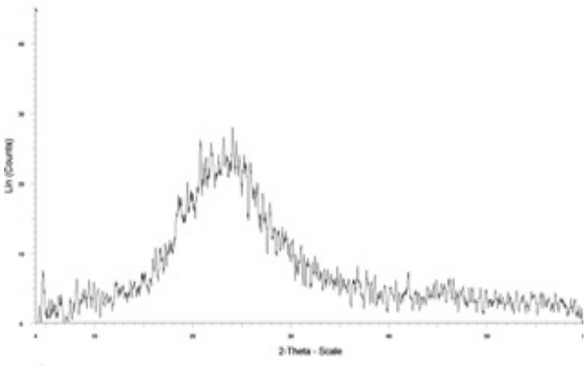

Fig. 2: XRD of BG

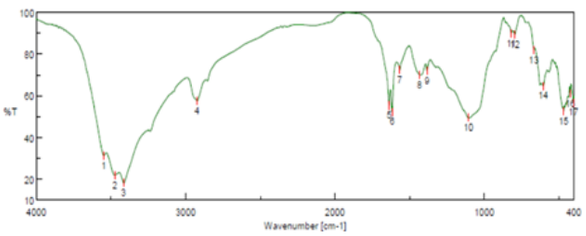

Fig. 3: FTIR of SiC /BG nanocomposite

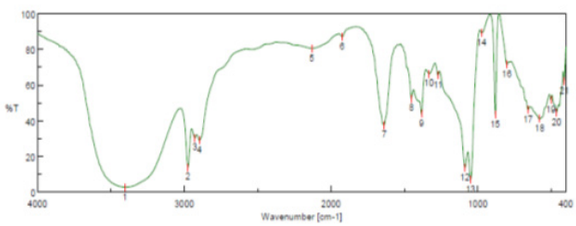

Fig. 4: FTIR of SiC /BG/ CMC nanocomposite

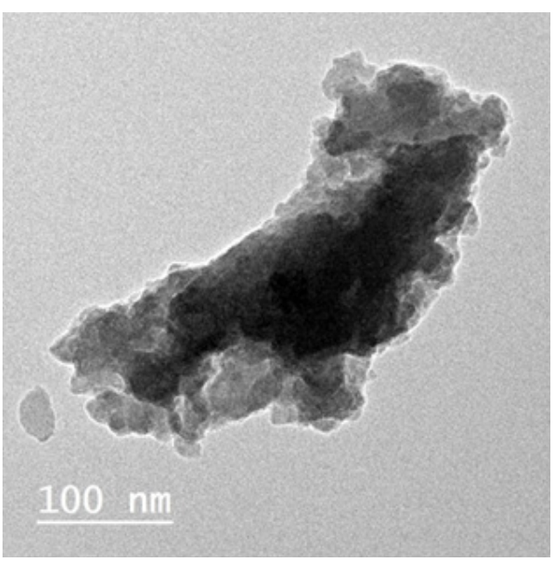

Fig. 5: TEM of SiC/BG nanocomposite

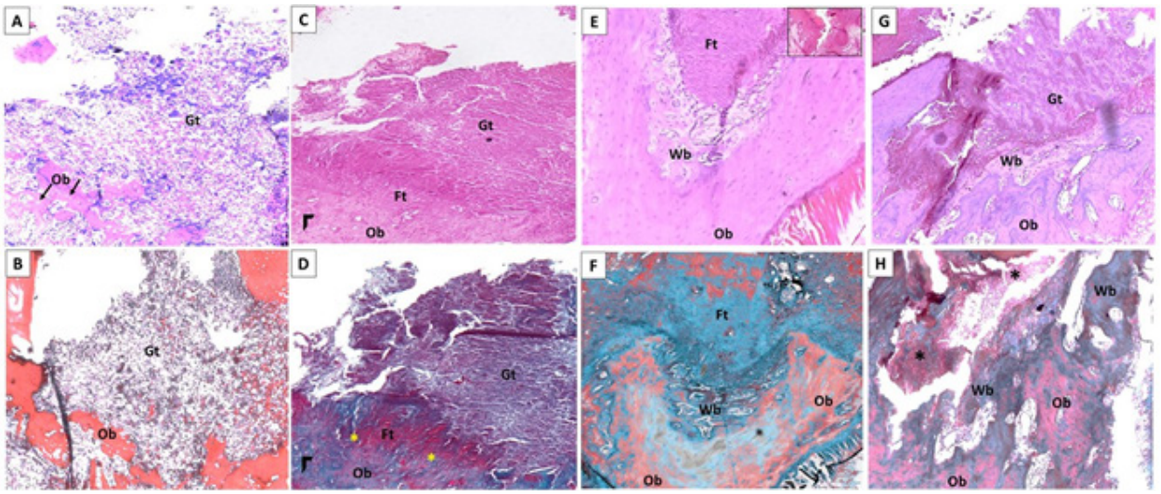

Fig. 6: A photomicrograph showing the healing socket 3 days after extraction. A, B: group Ia showed condensed area of granulation tissue (Gt), remnants of distorted old lamellar bone (Ob), widened osteolytic lacuna (black arrows). C, D: group IIa showing; granulation tissue (Gt), dense fibrous tissue (Ft) enclosing mature and immature collagen fibers, old lamellar bone (Ob). Thin network of newly formed immature bone (arrow head) E, F: group IIIa at the base of the socket showing; fibrous tissue (Ft), woven bone (Wb), old lamellar bone (Ob) Inset: showing mucosal regeneration. G, H: group IVa showing; granulation tissue (Gt), woven bone (Wb), remodeled old lamellar bone (Ob). Note: granulation tissue at the central and basal part of the socket (asterisks) (Figs.A,C,D,and G; H&E, Orig. Mag. 100) (Figs. B,D,F and H; Masson's trichrome, Orig. Mag. 100).

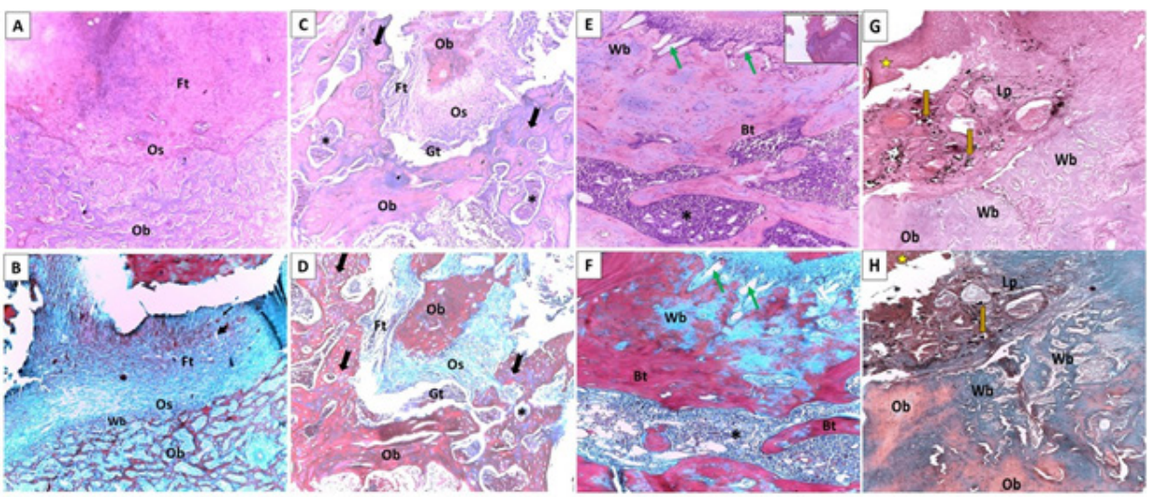

Fig. 7: A photomicrograph of all groups at 7 days after extraction. A, B: group Ib showing; fibrous tissue (Ft), osteoid matrix (Os), woven bone (Wb), old lamellar bone (Ob). C, D: group IIb showing; fibrous tissue (Ft), granulation tissue (Gt), osteoid matrix (Os), old lamellar bone (Ob), trabecular bone remodeling (notched arrows), bone marrow cavities (asterisks). E, F: group IIIb at the base of the socket showing; woven bone (Wb), mature bone trabeculae (Bt), numerous blood vessels (green arrows), cellular marrow cavities (asterisks). Inset: showing mucosal regeneration. G, H: group IVb showing; mucosal epithelium (star), lamina propria (Lp), remnants of the graft material (brown arrows), trabeculae of woven bone (Wb), old lamellar bone (Ob) (Figs.A,C,D,and G; H&E, Orig. Mag. 100) (Figs. B,D,F and H; Masson's trichrome, Orig. Mag. 100).

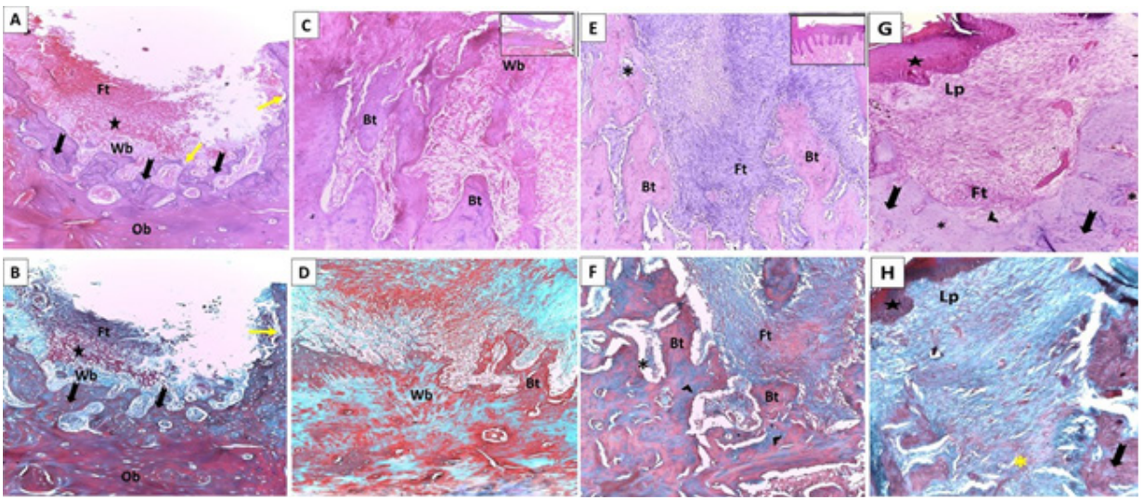

Fig. 8: A photomicrograph of all groups at 14 days after extraction. A, B: group Ic showing; dense fibrous tissue (Ft), mineralized bone matrix (star), woven bone (Wb), old lamellar bone (Ob), bone trabeculae remodeling (notched arrow heads), Howship's lacunae (yellow arrows). C, D: group IIc at the base of the socket showing; woven bone (Wb), irregular interconnecting bone trabeculae (Bt). Inset: showing mucosal regeneration. E, F: group IIIc at the base of the socket showing; dense fibrous tissue consists of mature and immature collagen fibers (Ft), mature bone trabeculae (Bt) with areas of immature bone (arrow heads), large marrow cavities (asterisks). Inset: showing mucosal regeneration. G, H: group IVc showing; mucosal epithelium (star), lamina propria (Lp), fibrous connective tissue (Ft), mature thick bone trabeculae (notched arrows), marrow cavities (black asterisks), discrete areas of immature bone trabeculae (arrow heads), mature collagen fibers (yellow asterisks). (Figs.A,C,D,and G; H&E, Orig. Mag. 100) (Figs. B,D,F and H; Masson's trichrome, Orig. Mag. 100).

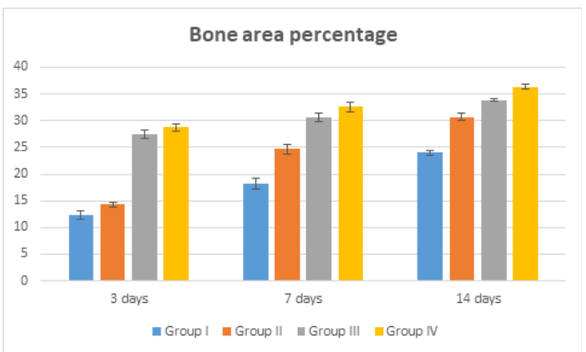

Fig. 9: Graph showing bone area percentage in different experimental groups within each experimental time interval. Data represent mean±SD. Columns shows mean values. Error bars correspond to SD

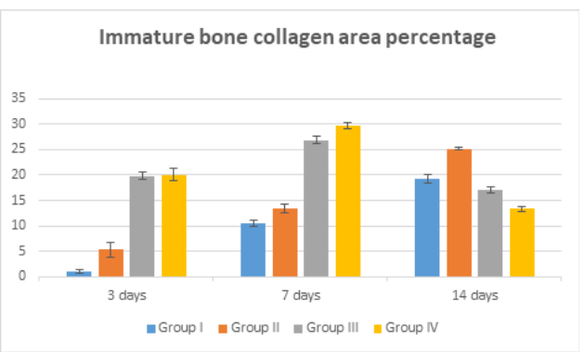

Fig. 10: Graph showing immature bone collagen area percentage in different experimental groups within each experimental time interval. Data represent mean±SD. Columns shows mean values. Error bars correspond to SD.

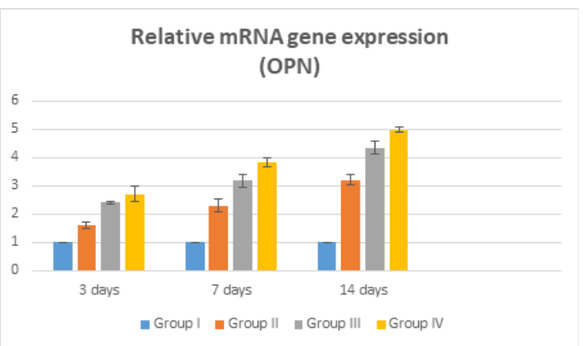

Fig. 11: Graph showing relative mRNA gene expression of OPN in different experimental groups within each experimental time interval. Data represent mean±SD. Columns shows mean values. Error bars correspond to SD

Table 2: Descriptive statistics and comparison between different experimental groups within each time interval for bone area percentage.

Parameter	Time interval	Experimental groups	Mean±SD	*P value*
Bone area percentage	3 days post extraction	Group Ia (control)	12.29±0.^{7}0^{C}	<0.00001*
		Group IIa (CMC)	14.25±0.52^{B}	
		Group IIIa (SiC/BG)	27.52±0.82^{A}	
		Group IVa (SiC/BG/CMC)	28.73±0.^{6}4^{A}	
	7 days post extraction	Group Ib (control)	18.25±1.03^{D}	<0.00001*
		Group IIb (CMC)	24.68±0.92^{C}	
		Group IIIb (SiC/BG)	30.55±0.79^{B}	
		Group IVb (SiC/BG/CMC)	32.58±0.90^{A}	
	14 days post extraction	Group Ic (control)	23.98±0.53^{D}	<0.00001*
		Group IIc (CMC)	30.64±0.70^{C}	
		Group IIIc (SiC/BG)	33.83±0.24^{B}	
		Group IVc (SiC/BG/CMC)	36.32±0.46^{A}	

Significance level $P<0.05$, * denotes significant difference between experimental groups using ANOVA test. Means with different superscript letters are significantly different using Post-hoc Tukey test.

Table 3: Descriptive statistics and comparison between different experimental groups within each time interval for immature bone collagen area percentage.

Parameter	Time interval	Experimental groups	Mean±SD	*P value*
Immaturebone collagen area percentage	3 days post extraction	Group Ia (control)	1.08±0.31^{C}	<0.00001*
		Group IIa (CMC)	5.282±1.51^{B}	
		Group IIIa (SiC/BG)	19.81±0.69^{A}	
		Group IVa (SiC/BG/CMC)	20.10±1.17^{A}	
	7 days post extraction	Group Ib (control)	10.53±0.52^{D}	<0.00001*
		Group IIb (CMC)	13.47±0.79^{C}	
		Group IIIb (SiC/BG)	26.85±0.69^{B}	
		Group IVb (SiC/BG/CMC)	29.66±0.60^{A}	
	14 days post extraction	Group Ic (control)	19.30±0.87^{B}	<0.00001*
		Group IIc (CMC)	25.15±0.28^{A}	
		Group IIIc (SiC/BG)	17.15±0.60^{C}	
		Group IVc (SiC/BG/CMC)	13.31±0.42^{D}	

Significance level $P<0.05$, * denotes significant difference between experimental groups using ANOVA test. Means with different superscript letters are significantly different using Post-hoc Tukey test.

Table 4: Descriptive statistics and comparison between different experimental groups within each time interval for OPN mRNA gene expression.

Parameter	Time interval	Experimental groups	Mean±SD	*P value*
OPN mRNA gene expression	3 days post extraction	Group Ia (control)	1±0^{D}	<0.00001*
		Group IIa (CMC)	1.61±0.11^{C}	
		Group IIIa (SiC/BG)	2.40±0.03^{B}	
		Group IVa (SiC/BG/CMC)	2.71±0.27^{A}	
	7 days post extraction	Group Ib (control)	1±0^{D}	<0.00001*
		Group IIb (CMC)	2.30±0.24^{C}	
		Group IIIb (SiC/BG)	3.17±0.24^{B}	
		Group IVb (SiC/BG/CMC)	3.84±0.16^{A}	
	14 days post extraction	Group Ic (control)	1±0^{D}	<0.00001*
		Group IIc (CMC)	3.2±0.18^{C}	
		Group IIIc (SiC/BG)	4.35±0.22^{B}	
		Group IVc (SiC/BG/CMC)	4.98±0.08^{A}	

Significance level $P<0.05$, * denotes significant difference between experimental groups using ANOVA test. Means with different superscript letters are significantly different using Post-hoc Tukey test.

DISCUSSION

The intricate and sequential process of extraction socket healing is an effort to preserve normal anatomical structure and function. Numerous studies have been conducted to improve this intricate process, such as using bone grafts or osteogenic medications to encourage bone repair[25,26]. The roles of various bioactive substances and their involvement in the various stages of wound healing have been clarified through recent developments in cellular and molecular biology. Fresh extraction socket wound healing dynamics have been influenced by the form of the bioactive substances that might be either a hydrogel formulation or a particle form[27,28].

The herein study was designed to assess the ability of a novel combination of silicon carbide/bioactive glass/ carboxymethyl chitosan (SiC/BG/CMC) nanocomposite to heal albino rat extraction sockets. This novel nanocomposite was compared to each of its constituent materials, carboxymethyl chitosan (CMC) and silicon carbide/bioactive glass (SiC/BG), to evaluate their combination effect.

In this experiment, male rats were of a choice because of the sex differences in hormonal status or gene expression. The female hormones, such as estrogen, was proved to affect bone metabolism so, male rats were selected to avoid any confounded results[29].

Nanotechnology has been shown to improve the mechanical and biological properties of the biomaterials. Nanoscale components exhibit higher cell proliferation, migration, and differentiation when compared to their counterparts[30,31]. Thus, the novel biocomposite used in this work was chosen to be in the nanoformulation.

Because of its biological and structural resemblance to real tissues, chitosan and its derivatives have become more and more popular among natural materials in bone tissue engineering[32]. Chitosan derivative; CMC was selected to be used in the present work due to its improved water solubility, gel-forming capacity and enhanced biological activities, such as biocompatibility, biodegradability, low immunogenicity, antimicrobial activity and antioxidant activity[33-35]. However, the degradation rate of CMC can be slow and unpredictable, which may pose challenges in applications requiring controlled degradation[6]. In addition, CMC hydrogels is mechanically weak if lacks cross-linkers, limiting their applicability in load-bearing biomedical applications. Incorporating cross-linkers has been shown to improve their mechanical properties[36].

In the present work, SiC was incorporated with BG to create a nanocomposite ceramic SiC/BG. This was based on earlier researches that showed each material's promising biological properties in the biomedical field. SiC bioceramic has been shown to have several benefits, such as biocompatibility, low inflammatory response, adverse tissue reaction, and non-reactivity to human body chemicals[37]. Surface reactivity and distinct chemical compositions have been used to describe BG. Because of their osteoconductive qualities and active role in regulating cellular function, they have been used as skeletal substitutes to successfully fill bone deficiencies in the oral cavity[38-40]. The addition of SiC to BG in this work also aimed to improve the mechanical properties of the resulting nanocomposite SiC/BG, since BG is known to have relatively low mechanical properties[41] and SiC is known to have great chemical and physical stability[42].

Addition of CMC to SiC/BG nano-composite material for bone healing was postulated to offer a synergistic approach to enhance the repair and regeneration process. SiC contributes mechanical strength and durability, mimicking the load-bearing properties of natural bone[42], while bioactive glass facilitates osteogenesis by releasing ions that stimulate bone cell activity and enhance the formation of hydroxyapatite, the mineral component of bone[40]. CMC adds biocompatibility and antibacterial properties that promote a conducive environment for healing and reduce the risk of infection[35]. Together, these materials create a multifunctional scaffold that supports structural integrity, accelerates bone tissue regeneration, and minimizes complications, making it a promising solution for advanced orthopedic applications.

Devices having hydrophilic surfaces are necessary for bone regeneration, tissue engineering (TE), and nanomedicine for better interaction with the biological environment. The BG based calcium silicate are characterized by hydrophilic structure on their surfaces when immersed in biological solutions or when implanted into bony defect[43]. In this framework, SiC/BG and SiC/ BG/CMC nanocomposite provide an appropriate platform for the development of biomaterials with unique properties for biological applications in bone regeneration.

At 3 days' post-extraction

In the present work histological results reported that the control (group Ia) showed granulation tissue and dense fibrous tissue with no evidence of newly formed collagen fibers seen in this group. It had been reported that granulation tissue, cell proliferation, and angiogenesis, are some of the early phases of the multi-step process of bone healing[44].

This group displayed evident widening of osteocyte lacunae proposed that mature osteocytes may utilize similar molecular mechanisms as osteoclasts to remove their perilacunar matrix, in a process called "osteocytic osteolysis"[45]. As the fact that osteocytes are highly mechanosensitive cells; mechanical stimulation of osteocytes can cause changes in their metabolic activity by producing signaling molecules like "Wingless-related integration site (Wnts)", "bone morphogenetic proteins (BMPs)", "nitric oxide (NO)", and "prostaglandin E2 (PGE2)", thereby adjusting the differentiation, recruitment, and action of osteoblasts and osteoclasts[46,47].

However, CMC group (group IIa) showed granulation tissue with much less evident inflammatory cellular infiltrate than the control group Ia, causing early beginning of the proliferative phase of bone healing in group IIa as the newly formed extracellular matrix promotes cellular migration, adhesion and anchorage[48].

The anti-inflammatory and the anti-oxidant properties of CMC may also contribute to the positive biological activity of CMC seen in this study. According to Schutters *et al*.,[49] and Ortega-Gómez *et al*.,[50], reducing inflammation at wound site provide a favorable microenvironment for other repair cells to play their role in wound healing. Resolution of inflammatory conditions is an active and coordinated process that result in restoration of tissue homeostasis, integrity and function. The antioxidant effect of CMC was found to be related to the hydroxyl and carboxyl groups in the polymer chain. They can easily absorb hydrogen atoms in free radicals and reactive oxygen species to form stable polymer groups. Thus, it can inhibit cell necrosis, elevates angiogenesis and increase blood flow which allows more nutrients transportation efficiently which is crucial to tissue regeneration[51].

Going through the present study's histological results, group IIIa (SiC/BG) demonstrated soft and hard tissue regeneration as early as 3 days' post-extraction as evidenced by formation of woven bone at the socket base as compared to both Ia and IIa groups. These findings may be owing to that the BG exhibits hydrophilic surface structures when submerged in biological fluids or inserted into bone defects. The biological environment is known to interact more effectively with hydrophilic surfaces[43]. BG offers a controlled ion release (e.g; Si, Ca, P and Na) and ion exchange process upon immersion in body fluid. Glass particles and the surrounding biological fluid first undergo an ionic exchange in which protons from the environment replace sodium that separates from the glass. In this manner, the wound's pH increases to neutral, fostering favorable conditions for healing and restoration. As the diffusion reaction proceeds, silica gel is created that will adhere to both soft and hard tissues, drawing in collagen fibers, chondroitin sulphate, and glycosaminoglycans. This gel layer is then integrated into the body and plays a vital part in the development of new tissue[52-55].

The phenomenon of widening of osteocyte lacunae is less evident in groups IIIa and IVa in this research. When glass particles contact with body fluids, it is plausible to assume that three reactions occur: diffusion, dissolution, and precipitation. Glass particles and the solution first undergo an ionic exchange in which protons from the surrounding environment replace sodium that separates from the glass. In this manner, the wound's pH changes from acidic to neutral, promoting healing, repair and reducing resorption[56].

Throughout histological analysis for sockets treated with SiC/BG/CMC (group IVa) in this study, newly formed woven bone as well as remodeled bone were evident in the base of the socket at 3 days' post-extraction. Statistical results demonstrated non-significant increase in bone area percentage and immature bone collagen percentage in SiC/BG/CMC (group IVa) as compared to SiC/BG (group IIIa), however this increase was significant as compared to both control (Ia) and CMC (IIa) group. This indicated that the effect of SiC/BG/CMC nanocomposite in stimulating early new bone formation outperformed control and CMC group, however it was comparable to SiC/BG group.

At 7 days' post-extraction

Both control (group Ib) and CMC (group IIb) showed dense fibrous connective tissue filling the center of the socket with vascularized osteoid tissue matrix. This's due to the fact that by the end of the first week, recruited mesenchymal stem cells (MSCs) differentiate into osteoblasts which begin synthesizing mineralized osteoid bone matrix. Concurrently, angiogenesis occurs, leading to the development of a vascularized network within the callus. This vascularization is critical for supplying the necessary nutrients and removing waste products, thereby supporting the maturation and mineralization of the osteoid matrix[57].

Bone remodeling in group IIb was clearly observed at the basal and the lateral portion of the socket which is in line with the fact that bundle bone is reported to be the first to be resorbed and replaced by woven bone, resulting in a significant decrease in bone height[58]. The biocompatibility and anti-inflammatory effect of CMC provide a beneficial environment to facilitate bone regeneration, thus, makes bone cells easy to grow, affect the "OPG/RANKL/RANK" signaling pathway, and promote osteogenesis[59,60]. In addition, Klokkevold *et al*.[61] studied the effect of chitosan on the differentiation of osteoblasts and bone formation in *vitro*, and the experimental findings demonstrated that chitosan might improve bone progenitor cell differentiation and encourage osteogenesis.

Immature woven bone was clearly seen in both group IIIb (SiC/BG) and group IVb (SiC/BG/CMC). The woven bone in group IVb enclosed numerous osteocytes as well as numerous marrow cavities filled with fibrocellular tissue. Areas of vascularization were clearly observed in both groups. Prior researches showed that all bioactive glass compositions might promote wound healing by enhancing fibroblast proliferation, granulation tissue growth and angiogenesis induction. Bioactive glass promotes endothelial cell proliferation, endothelial tubule development and fibroblast release of angiogenic growth factors[62,63].

These histological results were statistically supported as SiC/BG (group IIIb) showed a significant increase in mean bone area percentage, and OPN gene expression along all the observational time point intervals as compared to the control (Ib) and CMC groups (IIb). Meanwhile the SiC/BG/CMC (group IVb) showed a significant increase in bone area percentage at 7 days after extraction when compared to the SiC/BG (group IIIb). Comparing this increase to the

control (Ib) and CMC groups (IIb), it was still significant. Histologically, the formed bone trabeculae of SiC/BG/CMC (group IV) group appeared thick, organized and enclosed well defined marrow cavities.

At 14 days' post-extraction

In comparison to control group (Ic) in this work, soft tissue healing was evidenced in CMC (IIc) group by the presence of partial mucosal epithelial regeneration at 14 days' post-extraction. The reinforced role of CMC (IIc group) in production of collagen and acceleration of wound healing was previously confirmed. It was reported that CMC hydrogels, membranes and sponges all increased the expression of the marker protein "α-smooth muscle actin (α-SMA)", which distinguishes fibroblasts from myofibroblasts. Myofibroblasts have a greater capacity to secrete collagen fibers and can multiply quickly[35].

CMC positive healing effect observed in the present work might be related to the fact that chitosan and its derivative (CMC) contain a great number of amino groups. It interacts with various negatively charged proteins and glycolipids on the surface of red blood cells leading to activation of platelet adhesion, thus, achieving physiological hemostasis and promote angiogenesis. CMC has the capability of moisture absorption–retention, antimicrobial and emulsion stabilizing characteristics, thus, can interact with cells to promote cell adhesion, proliferation, differentiation, tissue regeneration, and wound healing[64-66].

Statistical analysis in this study revealed a significant increase in the mean bone area percentage, immature bone collagen percentage, and osteopontin gene expression in CMC group (group II) as compared to control group (group I) along the three experimental observational points suggesting that CMC promoted bone tissue regeneration. In accordance with the herein results, Liu *et al*.,[59] reported a greater amount of bone deposits and more bone formation around prosthesis in the CMC group of rabbits underwent total knee arthroplasty surgery. It was found that CMC effectively inhibited the inflammatory response and osteoclast activation and promote osteogenesis.

In comparison to the control (group I) and CMC (group II) groups in the current investigation, the extraction socket of SiC/BG (group III) group, showed enhanced pattern of bone deposition and maturation with full mucosal regeneration and full socket. These findings agreed with Ghanbari *et al*.,[67] who observed that SiC nanoparticles significantly increased fibroblast cell adhesion, viability and proliferation in *vitro*. Furthermore, Zhang *et al*.,[68] found that BG significantly accelerated skin wound healing in mice, with a higher daily closure rate and the best closing effect on the 15th day. BG also promoted angiogenesis and development toward normal tissues by inhibiting pyroptosis via Cx43/ROS signaling pathway. According to previous studies, the activation and upregulation of healing factors, such as "antigen haematopoietic form precursor" cluster of differentiation 44 (CD44), "fibroblast growth factor receptor precursor (N-sam)", "vascular cell adhesion protein precursor", "vascular endothelial growth factor (VEGF) precursor", and "fibronectin receptor beta subunit", are said to be part of BG's soft tissue healing mechanism[69,70]. Therefore, when exposed to such stimuli, the primary cells engaged in wound healing are stimulated to further multiply, develop and accumulate in regions close to the BG surface[73,71].

The bone regenerative ability of SiC/BG observed in this work, could be related to the bioactivity, biocompatibility and the osteoconductivity of this nanocomposite. In 2020, El-Ghannam *et al*.[72], noticed that a biomimetic calcium deficient carbonate layer containing hydroxyapatite was formed on SiC after two hours of immersion in simulated body fluid. It was reported that investigation of SiC in *vitro* after 7 days by scanning electron microscope (SEM) and molecular biology showed that MC3T3-E1 cells (immature osteoblast cell line) adhered to the SiC surface express osteocalcin after 14 days. Mineralized bone-like tissue was shown by FTIR examination of the extracellular matrix generated by the attached cells. These findings supported that SiC is osteoconductive and has the capacity to promote bone cell function and tissue creation.

Our histological results were statistically supported as SiC/BG (group III) showed a significant increase in mean bone area percentage, and OPN gene expression along all the observational time point intervals as compared to the control (group I) and CMC (group II) groups. Remarkably, by day 14, the SiC/BG (group III) group's immature bone collagen was significantly lower than that of the control (group I) and CMC (group II) groups, supporting the idea that bone maturation is progressing faster in group III.

This's in line with Tulyaganov *et al*.,[73], a clinically tested injectable paste consisting of BG and glycerol was injected into osseous lesions in rabbit femurs that were 2 mm in diameter and roughly 10 mm long. After a month, the experimental group's new bone development was more advanced than the control groups. At every stage of implantation, statistical analysis revealed a substantial difference between the experimental and control groups' intensity of bone development scores. The statistical significance of the "osteogenetic effect" indicates that this effect is real and not the result of chance.

Regarding The SiC/BG/CMC (group IV) group; complete epithelial healing with complete closure of socket cavity was observed. The formed bone trabeculae appeared thick, more organized and enclosed well defined marrow cavities as compared to other groups. According to Ribas *et al*.[74], in addition to allowing for protein absorption and cell attachment, the BG material's high reactive surface and the ions it released encourage bone marrow stem cells to differentiate into osteoblast-like cells with a significant amount of mineralized tissue formation, thus, supporting the formation of amorphous calcium phosphates or the hydroxyl apatite (HA) layer.

In the current work statistical evidence of increased area percentage of bone at 14 days in group IV might be

referred to combining SiC/BG nanocomposites and CMC that offered a synergistic effect among their mechanical properties, biocompatibility, and bioactivity. Natural polymers have generally been mixed with ceramic fillers to strengthen final system's structure and consequently, create composites with improved mechanical performance, thus, enhancing specific cellular response in the host, favoring regenerative process[75]. Pradhan *et al*.,[76] showed that the thermal stability, chemical resistance as well as tensile strength of chitosan were increased due to incorporation of SiC nanopowder. Similarly, the improved mechanical properties of chitosan/BG composites were brought about by the addition of BGs. The mechanical properties of the chitosan matrix were found to be enhanced by the BG surface's bond with the functional groups of the chitosan, which maintained the BG distributed throughout the matrix[77,78].

In line with findings obtained in the present work, Peter *et al*.,[79] stated that the addition of nano-BG to chitosan/gelatin scaffold significantly improved the adhesion and proliferation of MG-63 osteoblast-like cells. In another work, Wu & Li[80], reported that BG/ alginate/ CMC hydrogels showed higher bioactivity than alginate/ CMC hydrogels as they could accelerate wound healing by regulating the host inflammation responses, promoting angiogenesis and enhancing collagen deposition.

The presence of remnants of the used material in group III and IV may be owing to the presence of SiC in the composition of the material. Since SiC hardness and strong bonding characteristics render it resistant to degradation, unlike materials such as hydroxyapatite[81]. SiC's resistance to degradation makes it suitable for long-term in *vivo* applications, such as heart stent coatings and dental implants[82].

After correlating the overall results from the present study, it could be clearly demonstrated that extraction sockets treated with CMC, SiC/BG or SiC/BG/CMC exhibited better healing cascade regarding bone formation and maturation as well as soft tissue healing compared to the control untreated extraction sockets. Group IV (SiC/ BG/CMC) showed relatively the most regular well defined bone trabecula with a more regularly arranged osteocytes as compared to the other groups. Since construction of hybrid materials is a common and essential concept in tissue engineering, researches have aimed to develop scaffolds that closely replicate the properties of natural tissues[83], so, the hybrid biological materials that have been investigated in group IV have proved significant advantages in extraction socket healing over the use of single materials.

LIMITATIONS OF THE STUDY

Animal studies play a crucial role in evaluating bone healing, but they come with several limitations. One major limitation is the variations in bone regeneration rates, immune responses and metabolic processes among species which can lead to discrepancies in healing outcomes. While nanocomposites offer promising potential in bone healing, their application in animal studies presents several limitations such as achieving consistent biodegradation rates that match the natural bone remodeling process, potentially leading to incomplete integration or foreign body reactions. Ethical concerns also limit the extent of experiment that was conducted. While animal models provide valuable insights, their limitations highlight the need for alternative approaches such as in *vitro* models and computational simulations to complement in *vivo* research.

CONCLUSIONS AND RECOMMENDATIONS

Utilization of CMC into bone healing strategies demonstrates a notable improvement in the repair process compared to untreated group, owing to its biocompatibility, bioactivity and ability to support cellular functions and modulate inflammation. Regarding incorporation of SiC into BG scaffold, it has obviously a positive effect on the bone healing mechanism by enhancing the rate of the newly formed bone trabeculae and decreasing the inflammatory cell infiltrates. The mechanisms of action of CMC and SiC/BG in accelerating the bone healing process are different and the synergic effect of both materials are superior to using them separately. Addition of CMC to SiC/ BG enhance the biological and osteogenic properties of the material confirmed by the statistical analysis proving the superiority of novel combining noanocomposite. Further studies are recommended employed with a larger sample size, larger follow up period and further investigation tools. Also further bioassays and analysis are needed to characterize the structure and mechanism of the combined biomaterial (SiC/BG/CMC) nanocomposite to provide successful formulation of products for bone healing. The use of SiC/BG/CMC for acceleration of socket healing by definite dose and procedure needs further investigations.

ABBREVIATIONS

ANOVA: Multiple comparison analysis of variance, **BG:** Bioactive glass, **BMP:** Bone morphogenic protein, **CD44:** Cluster of differentiation 44, **CMC:** Carboxymethyl chitosan, **CS:** Chitosan, **CX43:** Connexin43, **Cx43:** Connexin 43, **EDTA:** Ethylenediamine tetraacetic acid, **FTIR:** Fourier-tranform infrared spectroscopy, **FTIR:** Fourier transform infrared spectroscopy, **GADPH:** Glyceraldehyde-3-phosphate dehydrogenase, **H&E:** Hematoxylin and Eosin, **HA:** Hydroxy apatite, **MSC:** Mesenchymal stem cells, **NaCaSi:** Sodium-Calcium-Silicate, **NaOH:** Sodium hydroxide, **NO:** Nitric Oxide, **N-sam:** Fibroblast growth factor receptor precursor, **OPG:** Osteoprotegerin, **OPN:** Osteopontin, **PGE2:** Prostaglandin E2, **qRT-PCR:** Reverse transcription polymerase chain reaction, **RANK:** Receptor activator of nuclear factor kappa B, **RANKL:** Receptor activator of nuclear factor kappa B ligand, **ROS:** Reactive oxygen species, **SEM:** Scanning electron microscope, **SiC:** Silicon carbide, **SMA:** Smooth muscle actin, **TE:** Tissue engineering, **TEM:** Transmission electron microscope, **TEOS:** Tetraethyl orthosilicate, **TPP:** Tri-polyphosphate, **VEGF:** Vascular endothelial

growth factor, **Wnt:** Wingless-related integration site, **XRD:** X-ray diffraction.

CONFLICT OF INTERETS

There are no conflicts of interest.

REFERENCES

1. Kashif, M., Mehmood, K., Ayub, T., & Aslam, M. (2014). Reasons and patterns of tooth extraction in a tertiary care hospital-A cross sectional prospective survey. J Liaquat Uni Med Health Sci, 13(03), 125-29. doi.org/10.3889/oamjms.2020.3784
2. Van der Weijden, F., Dell'Acqua, F., & Slot, D. E. (2009). Alveolar bone dimensional changes of post-extraction sockets in humans: a systematic review. Journal of clinical periodontology, 36(12), 1048-1058. doi.org/10.1111/j.1600-051X.2009.01482.x
3. Ten Heggeler, J. M. A. G., Slot, D. E., & Van der Weijden, G. A. (2011). Effect of socket preservation therapies following tooth extraction in non-molar regions in humans: a systematic review. Clinical oral implants research, 22(8), 779-788. doi.org/10.1111/j.1600-0501.2010.02064.x
4. Henry, C. (2016). The non-healing extraction socket: a diagnostic dilemma–case report and discussion. ISSN 0021-1133
5. Daigo, Y., Daigo, E., Hasegawa, A., Fukuoka, H., Ishikawa, M., & Takahashi, K. (2020). Utility of high-intensity laser therapy combined with photobiomodulation therapy for socket preservation after tooth extraction. Photobiomodulation, photomedicine, and laser surgery, 38(2), 75-83. doi.org/10.1089/photob.2019.4652
6. Mourya, V. K., Inamdar, N. N., & Tiwari, A. (2010). Carboxymethyl chitosan and its applications. Adv. Mater. Lett, 1(1), 11-33. doi: 10.5185/amlett.2010.3108
7. Gao, L., Yi, M., Xing, M., Li, H., Zhou, Y., Xu, Q.& Chang, J. (2020). In situ activated mesenchymal stem cells (MSCs) by bioactive hydrogels for myocardial infarction treatment. Journal of Materials Chemistry B, 8(34), 7713-7722. doi.org/10.1039/D0TB01320J
8. Gurumurthy, B., Pal, P., Griggs, J. A., & Janorkar, A. V. (2020). Optimization of collagen-elastin-like polypeptide-bioglass scaffold composition for osteogenic differentiation of adipose-derived stem cells. Materialia, 9, 100572. doi.org/10.1016/j.mtla.2019.100572
9. Mabrouk, M., Beherei, H. H., Shiomoto, S., Tanaka, Y., Osama, L., & Tanaka, M. (2023). Effect of titanium-doped bioactive glass on poly (2-hydroxyethyl methacrylate) hydrogel composites: Bioactivity, intermediate water, cell proliferation, and adhesion force. Ceramics International, 49(9), 13469-13481. doi.org/10.1016/j.ceramint.2022.12.221
10. Xu, M., Girish, Y. R., Rakesh, K. P., Wu, P., Manukumar, H. M., Byrappa, S. M., & Byrappa, K. (2021). Recent advances and challenges in silicon carbide (SiC) ceramic nanoarchitectures and their applications. Materials Today Communications, 28, 102533. doi.org/10.1016/j.mtcomm.2021.102533
11. Kenawy, S. H., Ali, A. F., Hamzawy, E. M. A., & Beherei, H. (2010). Sol-gel synthesis of wollastonite-phosphate compositions reinforced with nano-SiC ceramic for biomedical applications. Interceram, 59(5), 274-280. ISSN 00205214
12. Barroso, A., Mestre, H., Ascenso, A., Simões, S., & Reis, C. (2020). Nanomaterials in wound healing: From material sciences to wound healing applications. Nano Select, 1(5), 443-460. doi.org/10.1002/nano.202000055
13. Mabrouk, M., Rajendran, R., Soliman, I. E., Ashour, M. M., Beherei, H. H., Tohamy, K. M., ... & Das, D. B. (2019). Nanoparticle-and nanoporous-membrane-mediated delivery of therapeutics. Pharmaceutics, 11(6), 294. doi.org/10.3390/pharmaceutics11060294
14. Ladeira, N. M. B., Donnici, C. L., de Mesquita, J. P., & Pereira, F. V. (2021). Preparation and characterization of hydrogels obtained from chitosan and carboxymethyl chitosan. Journal of Polymer Research, 28(9), 335. doi.org/10.1007/s10965-021-02682-z
15. Rizvi, S. S. B., Akhtar, N., Minhas, M. U., Mahmood, A., & Khan, K. U. (2022). Synthesis and characterization of carboxymethyl chitosan nanosponges with cyclodextrin blends for drug solubility improvement. Gels, 8(1), 55. doi.org/10.3390/gels8010055
16. Akunna, C., & Cerruti, M. (2024). Structural connectivity and bioactivity in sol–gel silicate glass design. Acta Biomaterialia, 188, 374-392. doi.org/10.1016/j.actbio.2024.08.030
17. Nagasaki, R., Nagano, K., Nezu, T., & Iijima, M. (2023). Synthesis and characterization of bioactive glass and zinc oxide nanoparticles with enamel remineralization and antimicrobial capabilities. Materials, 16(21), 6878. doi.org/10.3390/ma16216878
18. Lairez, O., Lonjaret, L., Ruiz, S., Marchal, P., Franchitto, N., Calise, D.& Minville, V. (2013). Anesthetic regimen for cardiac function evaluation by echocardiography in mice: comparison between ketamine, etomidate and isoflurane versus conscious state. Laboratory animals, 47(4), 284-290. doi.org/10.1177/0023677213496236
19. Paramitha, D., Ulum, M. F., Purnama, A., Wicaksono, D. H. B., Noviana, D., & Hermawan, H. (2017). Monitoring degradation products and metal ions in *vivo*. In Monitoring and evaluation of biomaterials and their performance in *vivo* (pp. 19-44). Woodhead Publishing. doi.org/10.1016/B978-0-08-100603-0.00002-X

20. Ahmed, A. I., El Agaty, S. M., & El-Sayed, S. M. (2024). Histological and Morphometric Study on the Effect of Triiodothyronine on the Histological Changes of Gastrocnemius Muscle of Aged Male Albino Rat Associated with Thyroid Dysfunction. Egyptian Journal of Histology, 47(1), 77-94. dx.doi.org/10.21608/ejh.2022.162526.1774

21. Abd Allah, F. M., Moustafa, A. M., Moahmmed, L. S., & Abd Allah, E. E. D. E. (2020). Histological and immunohistochemical studies on the role of stem cells on the burned skin of adult male albino rats. International Journal of Medical Arts, 2(1), 265-291. dx.doi.org/10.21608/ijma.2020.20386.1050

22. Hartig, S. M. (2013). Basic image analysis and manipulation in ImageJ. Current protocols in molecular biology, 102(1), 14-15. doi.org/10.1002/0471142727.mb1415s102

23. Artika, I. M., Dewi, Y. P., Nainggolan, I. M., Siregar, J. E., & Antonjaya, U. (2022). Real-time polymerase chain reaction: current techniques, applications, and role in COVID-19 diagnosis. Genes, 13(12), 2387. doi.org/10.3390/genes13122387

24. Chan, Y. H. (2003). Biostatistics 102: quantitative data–parametric & non-parametric tests. blood Press, 140(24.08), 79. PMID: 14700417 ISSN 0037-5675

25. Dimitriou, R., Mataliotakis, G. I., Angoules, A. G., Kanakaris, N. K., & Giannoudis, P. V. (2011). Complications following autologous bone graft harvesting from the iliac crest and using the RIA: a systematic review. Injury, 42, S3-S15. doi.org/10.1016/j.injury.2011.06.015

26. Chandran, S., Babu S, S., VS, H. K., Varma, H. K., & John, A. (2016). Osteogenic efficacy of strontium hydroxyapatite micro-granules in osteoporotic rat model. Journal of biomaterials applications, 31(4), 499-509. doi.org/10.1177/0885328216647197

27. Matin, K., Nakamura, H., Irie, K., Ozawa, H., & Ejiri, S. (2001). Impact of recombinant human bone morphogenetic protein-2 on residual ridge resorption after tooth extraction: an experimental study in the rat. International Journal of Oral & Maxillofacial Implants, 16(3). doi.org/10.2186/jjps.47.662

28. Hahn, J., Rohrer, M. D., & Tofe, A. J. (2003). Clinical, radiographic, histologic, and histomorphometric comparison of PepGen P-15 particulate and PepGen P-15 flow in extraction sockets: a same-mouth case study. Implant Dentistry, 12(2), 170-174. doi.org/10.1097/01.ID.0000064812.39660.FF

29. Hegazy, A. A., Qenawy, N. M., Abdel Aziz, N. M., & El-Bestawy, E. M. (2023). Possible protective role of capsaicin against high fat diet effects on liver and gall bladder of adult male mice. Egyptian Journal of Histology, 46(1), 245-262. dx.doi.org/10.21608/ejh.2021.92731.1558

30. Du, R. L., Chang, J., Ni, S. Y., Zhai, W. Y., & Wang, J. Y. (2006). Characterization and in *vitro* bioactivity of zinc-containing bioactive glass and glass-ceramics. Journal of biomaterials applications, 20(4), 341-360. doi.org/10.1177/0885328206054535

31. Hu, Q., Tang, H., Wu, H., Xu, Y., Li, W., Wang, X. & Liu, J. (2024). Facile synthesis, characterization, biocompatibility and protein loading/release property of zinc-doped hollow mesoporous bioactive glass nanospheres. Journal of Sol-Gel Science and Technology, 110(2), 518-531. doi.org/10.1007/s10971-024-06374-0

32. Mostafa, A. A., El-Sayed, M. M., Mahmoud, A. A., & Gamal-Eldeen, A. M. (2017). Bioactive/natural polymeric scaffolds loaded with ciprofloxacin for treatment of osteomyelitis. AAPS PharmSciTech, 18, 1056-1069. doi.org/10.1208/s12249-016-0605-0

33. de Abreu, F. R., & Campana-Filho, S. P. (2009). Characteristics and properties of carboxymethylchitosan. CarbohydratePolymers, 75(2),214-221. doi.org/10.1016/j.carbpol.2008.06.009

34. Upadhyaya, L., Singh, J., Agarwal, V., & Tewari, R. P. (2013). Biomedical applications of carboxymethylchitosans. Carbohydratepolymers, 91(1),452-466.doi.org/10.1016/j.carbpol.2012.07.076

35. Wang, D., Zhang, N., Meng, G., He, J., & Wu, F. (2020). The effect of form of carboxymethyl-chitosan dressings on biological properties in wound healing. Colloids and Surfaces B: Biointerfaces, 194, 111191. doi.org/10.1016/j.colsurfb.2020.111191

36. Kłosiński, K. K., Wach, R. A., Girek-Bąk, M. K., Rokita, B., Kołat, D., Kałuzińska-Kołat, Ż. & Pasieka, Z. W. (2022). Biocompatibility and mechanical properties of carboxymethyl chitosan hydrogels. Polymers, 15(1), 144. doi.org/10.3390/polym15010144

37. Xu, M., Girish, Y. R., Rakesh, K. P., Wu, P., Manukumar, H. M., Byrappa, S. M., & Byrappa, K. (2021). Recent advances and challenges in silicon carbide (SiC) ceramic nanoarchitectures and their applications. Materials Today Communications, 28, 102533. doi.org/10.1016/j.mtcomm.2021.102533

38. Mengel, R., Schreiber, D., & Flores-de-Jacoby, L. (2006). Bioabsorbable membrane and bioactive glass in the treatment of intrabony defects in patients with generalized aggressive periodontitis: results of a 5-year clinical and radiological study. Journal of periodontology, 77(10), 1781-1787. doi.org/10.1902/jop.2006.060029

39. Leu, A., & Leach, J. K. (2008). Proangiogenic potential of a collagen/bioactive glass substrate. Pharmaceutical research, 25, 1222-1229. doi.org/ 10.1007/s11095-007-9508-9

40. Skallevold, H. E., Rokaya, D., Khurshid, Z., & Zafar, M. S. (2019). Bioactive glass applications in dentistry. International journal of molecular sciences, 20(23), 5960. doi.org/10.3390/ijms20235960

41. Park, J., Na, H., Choi, S. C., & Kim, H. J. (2019). Biocompatibility of 13-93 bioactive glass-SiC fabric composites. Journal of the Korean Ceramic Society, 56(2). doi.org/10.4191/kcers.2019.56.2.12

42. Li, T., Li, X. L., Hu, S. X., & Wu, J. (2019). Enhanced osteoporotic effect of silicon carbide nanoparticles combine with nano-hydroxyapatite coated anodized titanium implant on healthy bone regeneration in femoral fracture. Journal of Photochemistry and Photobiology B: Biology, 197, 111515. doi.org/10.1016/j.jphotobiol.2019.111515

43. Ghiasi, M. S., Chen, J. E., Rodriguez, E. K., Vaziri, A., & Nazarian, A. (2019). Computational modeling of human bone fracture healing affected by different conditions of initial healing stage. BMC musculoskeletal disorders, 20, 1-14. doi.org/10.1186/s12891-019-2854-z

44. Tsourdi, E., Jähn, K., Rauner, M., Busse, B., & Bonewald, L. F. (2018). Physiological and pathological osteocytic osteolysis. Journal of musculoskeletal & neuronal interactions, 18(3), 292. PMID: 30179206 PMCID: PMC6146198

45. Robling, A. G., Niziolek, P. J., Baldridge, L. A., Condon, K. W., Allen, M. R., Alam, I., ... & Turner, C. H. (2008). Mechanical stimulation of bone in *vivo* reduces osteocyte expression of Sost/sclerostin. Journal of Biological Chemistry, 283(9), 5866-5875. doi.org/10.1074/jbc.M705092200

46. Kulkarni, R. N., Bakker, A. D., Everts, V., & Klein-Nulend, J. (2010). Inhibition of osteoclastogenesis by mechanically loaded osteocytes: involvement of MEPE. Calcified tissue international, 87(5), 461-468. doi.org/10.1007/s00223-010-9407-7

47. Pagni, G., Pellegrini, G., Giannobile, W. V., & Rasperini, G. (2012). Postextraction alveolar ridge preservation: biological basis and treatments. International journal of dentistry, 2012(1), 151030. doi.org/10.1155/2012/151030

48. Schutters, K., Kusters, D. H., Chatrou, M. L., Montero-Melendez, T., Donners, M., Deckers, N. M. & Reutelingsperger, C. P. (2013). Cell surface-expressed phosphatidylserine as therapeutic target to enhance phagocytosis of apoptotic cells. Cell Death & Differentiation, 20(1), 49-56. doi.org/10.1038/cdd.2012.107

49. Ortega-Gómez, A., Perretti, M., & Soehnlein, O. (2013). Resolution of inflammation: an integrated view. EMBO molecular medicine, 5(5), 661-674. doi.org/10.1002/emmm.201202382

50. Ramasamy, P., Subhapradha, N., Thinesh, T., Selvin, J., Selvan, K. M., Shanmugam, V., & Shanmugam, A. (2017). Characterization of bioactive chitosan and sulfated chitosan from Doryteuthis singhalensis (Ortmann, 1891). International journal of biological macromolecules, 99, 682-691. doi.org/10.1016/j.ijbiomac.2017.03.041

51. Mabrouk, M., Mousa, S. M., Shalaby, M. B., Shalby, A. B., Beherei, H. H., & Das, D. B. (2023). Egyptian corals-based calcium silicate (CaS) nanopowders doped with zinc/copper for improved chemical stability and treatment of calvarial defects. Colloids and Surfaces A: Physicochemical and Engineering Aspects, 660, 130875. doi.org/10.1016/j.colsurfa.2022.130875

52. Hamadouche, M., & Sedel, L. (2000). Ceramics in orthopaedics. The Journal of Bone & Joint Surgery British Volume, 82(8), 1095-1099. doi.org/10.1302/0301-620X.82B8.0821095

53. Macedo, N. L. D., Matuda, F. D. S., Macedo, L. G. S. D., Gonzales, M. B., Ouchi, S. M., & Carvalho, Y. R. (2004). Bone defect regeneration with bioactive glass implantation in rats. Journal of Applied Oral Science, 12, 137-143. doi.org/10.1590/S1678-77572004000200011

54. Eraba, K. M. T., Khedr, E. G., Atia, T. A., & Mourad, S. E. (2007). Histological Study Of The Influence Of Bioactive Glass On Bone Healing (An Experimental Study On Rat Femur). The Egyptian Journal of Hospital Medicine, 29(1), 672-684. dx.doi.org/10.21608/ejhm.2007.17709

55. Öksüz, K. E. (2024). Bioactive coatings on biopolymer materials: evaluation of mechanical, physical, thermal, and in *vitro* properties. Journal of the Australian Ceramic Society, 60(4), 1265-1280. doi.org/10.1007/s41779-024-01037-3

56. Shapoff, C. A., Alexander, D. C., & Clark, A. E. (1997). Clinical use of a bioactive glass particulate in the treatment of human osseous defects. Compendium of continuing education in dentistry (Jamesburg, NJ: 1995), 18(4), 352-4. PMID: 9452543

57. Marsell, R., & Einhorn, T. A. (2011). The biology of fracture healing. Injury, 42(6), 551-555. doi.org/10.1016/j.injury.2011.03.031

58. Araújo, M. G., & Lindhe, J. (2005). Dimensional ridge alterations following tooth extraction. An experimental study in the dog. Journal of clinical periodontology, 32(2), 212-218. doi.org/10.1111/j.1600-051X.2005.00642.x

59. Liu, F., Li, H. Y., Wang, Z., Zhang, H. N., Wang, Y. Z., & Xu, H. (2020). Carboxymethyl chitosan reduces inflammation and promotes osteogenesis in a rabbit knee replacement model. BMC Musculoskeletal Disorders, 21, 1-10. doi.org/10.1186/s12891-020-03803-3

60. Li, M., Xu, L., Ma, F., Tang, B., & Qin, C. (2023). Fabrication of carboxymethyl chitosan-strontium chondroitin sulfate composites for potential bone regeneration. Polymer Testing, 123, 108053. doi.org/10.1016/j.polymertesting.2023.108053

61. Klokkevold, P. R., Vandemark, L., Kenney, E. B., & Bernard, G. W. (1996). Osteogenesis enhanced by chitosan (poly-N-acetyl glucosaminoglycan) in *vitro*. Journal of periodontology, 67(11), 1170-1175. doi.org/10.1902/jop.1996.67.11.1170

62. Moosvi, S. R., & Day, R. M. (2009). Bioactive glass modulation of intestinal epithelial cell restitution. Acta Biomaterialia, 5(1), 76-83. doi.org/10.1016/j.actbio.2008.08.003

63. Balasubramanian, P., Hupa, L., Jokic, B., Detsch, R., Grünewald, A., & Boccaccini, A. R. (2017). Angiogenic potential of boron-containing bioactive glasses: in *vitro* study. Journal of Materials Science, 52, 8785-8792. doi.org/10.1007/s10853-016-0563-7

64. Fan, L., Yang, J., Wu, H., Hu, Z., Yi, J., Tong, J., & Zhu, X. (2015). Preparation and characterization of quaternary ammonium chitosan hydrogel with significant antibacterial activity. International journal of biological macromolecules, 79, 830-836. doi.org/10.1016/j.ijbiomac.2015.04.013

65. Kyzas, G. Z., & Bikiaris, D. N. (2015). Recent modifications of chitosan for adsorption applications: a critical and systematic review. Marine drugs, 13(1), 312-337. doi.org/10.3390/md13010312

66. Fiamingo, A., & Campana-Filho, S. P. (2016). Structure, morphology and properties of genipin-crosslinked carboxymethylchitosan porous membranes. Carbohydrate polymers, 143, 155-163. doi.org/10.1016/j.carbpol.2016.02.016

67. Ghanbari, M., Salavati-Niasari, M., Mohandes, F., & Firouzi, Z. (2022). Modified silicon carbide NPs reinforced nanocomposite hydrogels based on alginate-gelatin by with high mechanical properties for tissue engineering. Arabian Journal of Chemistry, 15(1), 103520. doi.org/10.1016/j.arabjc.2021.103520

68. Zhang, K., Chai, B., Ji, H., Chen, L., Ma, Y., Zhu, L. & Xu, K. (2022). Bioglass promotes wound healing by inhibiting endothelial cell pyroptosis through regulation of the connexin 43/reactive oxygen species (ROS) signaling pathway. Laboratory Investigation, 102(1), 90-101. doi.org/10.1038/s41374-021-00675-6

69. Xynos, I. D., Edgar, A. J., Buttery, L. D., Hench, L. L., & Polak, J. M. (2001). Gene-expression profiling of human osteoblasts following treatment with the ionic products of Bioglass® 45S5 dissolution. Journal of Biomedical Materials Research: An Official Journal of The Society for Biomaterials, The Japanese Society for Biomaterials, and The Australian Society for Biomaterials and the Korean Society for Biomaterials, 55(2), 151-157.doi.org/10.1002/1097-4636(200105)55:2%3C151::AID-JBM1001%3E3.0.CO;2-D

70. Yu, H., Peng, J., Xu, Y., Chang, J., & Li, H. (2016). Bioglass activated skin tissue engineering constructs for wound healing. ACS applied materials & interfaces, 8(1), 703-715. doi.org/10.1021/acsami.5b09853

71. Zhou, J., Wang, H., Zhao, S., Zhou, N., Li, L., Huang, W.& Zhang, C. (2016). In *vivo* and in *vitro* studies of borate based glass micro-fibers for dermal repairing. Materials Science and Engineering: C, 60, 437-445. doi.org/10.1016/j.msec.2015.11.068

72. El-Ghannam, A., Greenier, M., Johnson, M., & Marriott, I. (2020). Synthesis and characterization of porous bioactive SiC tissue engineering scaffold. Journal of Biomedical Materials Research Part A, 108(11), 2162-2174. doi.org/10.1002/jbm.a.36973

73. Tulyaganov, D. U., Akbarov, A., Ziyadullaeva, N., Khabilov, B., & Baino, F. (2020). Injectable bioactive glass-based pastes for potential use in bone tissue repair. Biomedical glasses, 6(1), 23-33. doi.org/10.1515/bglass-2020-0003

74. Ribas, R. G., Schatkoski, V. M., do Amaral Montanheiro, T. L., de Menezes, B. R. C., Stegemann, C., Leite, D. M. G., & Thim, G. P. (2019). Current advances in bone tissue engineering concerning ceramic and bioglass scaffolds: A review. Ceramics International, 45(17), 21051-21061. doi.org/10.1016/j.ceramint.2019.07.096

75. Rao, S. H., Harini, B., Shadamarshan, R. P. K., Balagangadharan, K., & Selvamurugan, N. (2018). Natural and synthetic polymers/bioceramics/bioactive compounds-mediated cell signalling in bone tissue engineering. International journal of biological macromolecules, 110, 88-96. doi.org/10.1016/j.ijbiomac.2017.09.029

76. Pradhan, G. C., Dash, S., & Swain, S. K. (2015). Barrier properties of nano silicon carbide designed chitosan nanocomposites. Carbohydrate polymers, 134, 60-65. doi.org/10.1016/j.carbpol.2015.06.081

77. Couto, D. S., Hong, Z., & Mano, J. F. (2009). Development of bioactive and biodegradable chitosan-based injectable systems containing bioactive glass nanoparticles. Acta Biomaterialia, 5(1), 115-123. doi.org/10.1016/j.actbio.2008.08.006

78. Caridade, S. G., Merino, E. G., Alves, N. M., de Zea Bermudez, V., Boccaccini, A. R., & Mano, J. F. (2013). Chitosan membranes containing micro or nano-size bioactive glass particles: evolution of biomineralization followed by in situ dynamic mechanical analysis. journal of the mechanical behavior of biomedical materials, 20, 173-183. doi.org/10.1016/j.jmbbm.2012.11.012

79. Peter, M., Binulal, N. S., Nair, S. V., Selvamurugan, N., Tamura, H., & Jayakumar, R. (2010). Novel biodegradable chitosan–gelatin/nano-bioactive glass ceramic composite scaffolds for alveolar bone tissue engineering. Chemical engineering journal, 158(2), 353-361. doi.org/10.1016/j.cej.2010.02.003

80. Wu, X., & Li, H. (2021). Incorporation of bioglass improved the mechanical stability and bioactivity of alginate/carboxymethyl chitosan hydrogel wound dressing. ACS applied bio materials, 4(2), 1677-1692. doi.org/10.1021/acsabm.0c01477

81. Santavirta, S., Takagi, M., Nordsletten, L., Anttila, A., Lappalainen, R., & Konttinen, Y. T. (1998). Biocompatibility of silicon carbide in colony formation test in *vitro*: a promising new ceramic THR implant coating material. Archives of orthopaedic and trauma surgery, 118, 89-91. doi.org/10.1007/s004020050319

82. Saddow, S. E. (2022). Silicon Carbide Technology for Advanced Human Healthcare Applications. Micromachines 2022, 13, 346. doi.org/10.3390/mi13030346

83. Casarin, M., Todesco, M., Fontanella, C. G., Morlacco, A., Dal Moro, F., & Bagno, A. (2023). Hybrid materials for tissue repair and replacement: another frontier in biomaterial exploitation focusing on cardiovascular and urological fields. Processes, 11(7), 2013. doi.org/10.3390/pr11072013

الملخص العربى

تقييم إمكانات الشفاء لمركبات النانو للكربيد السيليكون/الزجاج النشط بيولوجياً/ الكربوكسي كيثيل الكيتوزان على مغرز الاقتلاع في الجرذان البيضاء

مي رجب[١]، دينا فرج[١]، زينب سالم[١،٢]، حنان بحيري[٣]، سحر محمد شوكت[١]

[١]قسم بيولوجيا الفم، كلية طب الأسنان، جامعة القاهرة، مصر.

[٢]كلية طب الفم والأسنان، جامعة ٦ أكتوبر، الجيزة، مصر.

[٣]قسم السيراميك ومواد البناء، معهد بحوث تكنولوجيا المواد المتقدمة والثروة المعدنية، المركز القومي للبحوث.

مقدمه: يعتبر خلع الأسنان من أكثر الإجراءات السنية انتشارًا. حيث تم الإبلاغ عن أن العيب السنخي الناتج عن خلع الأسنان يبلغ حوالي ١١٪.

الهدف من البحث: هو تقييم إمكانات الشفاء من مركبات النانو كربيد السيليكون / الزجاج الحيوي / كربوكسي ميثيل الكيتوزان على تجويف الخلع للفئران البيضاء.

مواد وطرق البحث : تم استخدام ٣٦ من ذكور الجرذان البيضاء في هذه الدراسة. تم استخراج الأضراس السفلية الأولى من كلا الجانبين. تم توزيع الجرذان عشوائيًا إلى أربع مجموعات، المجموعة الاولي)المجموعة الضابطة(بدون أي علاج، المجموعة الثانية : مجموعة كربوكسي ميثيل كيتوزان CMC) ، المجموعة الثالثة: مجموعة كربيد السيليكون/الزجاج النشط بيولوجيًا SiC/BG) (والمجموعة الرابعة : مجموعة كربيد السيليكون/الزجاج النشط بيولوجيًا/كربوكسي ميثيل كيتوزان SiC/BG/CMC). (تم تقسيم كل مجموعة وفقًا لتاريخ التضحية ٣ و ٧ و ١٤ يومًا إلى ثلاث مجموعات فرعية. تم تقييم فعالية المواد العلاجية نسيجيًا وهستومورفومتريًا وباستخدام تفاعل البوليميراز المتسلسل في الوقت الحقيقي (qRT-PCR) للتحليل الكمي للتعبير الجيني عن أوستيوبونتين (OPN). تم إجراء تحليل إحصائي لجميع البيانات.

النتائج: أظهرت النتائج النسيجية أن المجموعة الأولى أظهرت معدل شفاء أبطأ من المجموعات الأخرى. أظهرت المجموعة الثانية سلسلة شفاء أفضل من المجموعة الأولى. أظهرت المجموعة الثالثة والمجموعة الرابعة بشكل عام شفاء أفضل مع تكوين عظام جديدة أكثر من المجموعات الأخرى في فترات زمنية مختلفة. تم تسجيل زيادة كبيرة في نسبة مساحة العظام المشكلة حديثًا في المجموعة الرابعة على طول فترات تجريبية مختلفة. تم الكشف عن أعلى نسبة مساحة للعظام عند ١٤ يومًا فيما يتعلق بالمجموعات الرابعة والثالثة والأولى، بينما في المجموعة الثانية لم يكن هناك فرق كبير إحصائيًا في كلتا الفترتين الزمنيتين: ٧ و ١٤ يومًا. كشفت نتائج qRT-PCR عند فترة ٣ و ٧ أيام عن زيادة كبيرة في مستوى OPN في المجموعة الثانية، بينما عند فترة ١٤ يومًا؛ تم الكشف عن أعلى مستوى OPN في المجموعة الرابعة تليها المجموعة الثالثة.

خلاصة البحث: أظهرت المجموعة الرابعة نتائج متفوقة حيث تم تكوين المزيد من العظام الجديدة مع خلايا عظمية مرتبة بشكل أكثر انتظامًا مقارنة بالمجموعات الأخرى.